Robust Secondary Frequency Control for Virtual Synchronous Machine-Based Microgrid Cluster Using Equivalent Modeling

Wenqiang Hu, *Student Member, IEEE*, Zaijun Wu, *Member, IEEE*, Xinxin Lv, *Student Member, IEEE*, and Venkata Dinavahi, *Fellow, IEEE*

***Abstract*—The technology of virtual synchronous machine (VSM) is attracting interest of researchers as it controls converters mimicking the synchronous machine's response so as to provide inertial support for power electronics dominated smart grids. For the VSM-based microgrid, its slow dynamics are dominated by synchronous generators (SGs) and the VSM control loops, which makes it possible to model this microgrid into an equivalent SG (EqSG) model. This paper proposes a robust secondary frequency control design method for the VSM-based low voltage (LV) microgrid cluster (MGC) using equivalent modeling. The EqSG model is used to construct the MGC model so as to reduce the model order and the complexity of controller synthesis. Modeling errors caused by the EqSG model and different operating conditions are integrated into the MGC model as unstructured uncertainties. The proposed secondary frequency control strategy is based on the distributed-centralized hybrid control structure to coordinate frequency restoration among LV microgrids. Structured μ-synthesis is applied for tuning control parameters realizing H_∞ robust performance against unstructured uncertainties. To reduce the communication resource consumption, an event-triggered mechanism considering communication delay is introduced in the robust secondary frequency control strategy. The triggering condition is analyzed using a Lyapunov function to guarantee H_∞ robust stability. Simulation and real-time experiment results on a MGC composed of four CIGRÉ benchmark LV microgrids are presented to demonstrate the effectiveness of the proposed control strategy.**

***Index Terms*—Event-triggered mechanism, H_∞ robust control, microgrid cluster, microgrid equivalent modeling, secondary frequency control, virtual synchronous machine.**

Manuscript received September 23, 2020; revised February 5, 2021; accepted March 15, 2021. Date of publication March 19, 2021; date of current version June 21, 2021. This work was supported in part by the National Natural Science Foundation of China under Grant 51977034; in part by the National Key Research and Development Program of China under Grant 2016YFB0900504; and in part by the Natural Science and Engineering Research Council of Canada (NSERC). The work of Wenqiang Hu was supported by China Scholarship Council (CSC). Paper no. TSG-01440-2020. *(Corresponding author: Zaijun Wu.)*

Wenqiang Hu and Zaijun Wu are with the School of Electrical Engineering, Southeast University, Nanjing 210096, China (e-mail: wqhu@seu.edu.cn; zjwu@seu.edu.cn).

Xinxin Lv is with the College of Energy and Electrical Engineering, Hohai University, Nanjing 210098, China (e-mail: xinxinlvhhuc@163.com).

Venkata Dinavahi is with the Department of Electrical and Computer Engineering, University of Alberta, Edmonton, AB T6G 2V4, Canada (e-mail: dinavahi@ualberta.ca).

Color versions of one or more figures in this article are available at https://doi.org/10.1109/TSG.2021.3067317.

Digital Object Identifier 10.1109/TSG.2021.3067317

I. Introduction

With small-scale renewable energy sources (RES) integrating into distribution networks, modern power systems are experiencing a paradigm shift from centralized generation and top-down structure to distributed generation and bottom-up structure, intensifying the distribution network operating as an interconnected multi-microgrids system, i.e., a microgrid cluster (MGC) [1]. However, the lack of sufficient inertia deteriorates frequency stability in the MGC. To deal with this challenge, the technology of virtual synchronous machine (VSM) was proposed and applied in distributed generation units (DGUs), energy storage units (ESUs) and controllable loads (CLs) [2], [3]. Even though aforementioned VSM control strategies are slightly different from each other, the principles are similar that most of them emulate the fundamental swing equation of synchronous machines in their power control loops, so as to synchronize with the grid frequency and provide virtual inertia in microgrids [4]. However, the steady-state response of the VSM exhibits frequency and voltage droop characteristics, which requires additional level of control to restore frequency and voltage to nominal values. To deal with this problem, most microgrids apply the hierarchical control structure [5], where the VSM control belongs to the primary level, the secondary level restores frequency and voltage to nominal values within a single microgrid, and the tertiary level is responsible for economic dispatch and power flow optimization among microgrids. As for a MGC, the voltage restoration can be realized by the secondary level within each microgrid locally, but the frequency restoration should be reconsidered over the whole MGC as the frequency is coupled and synchronized among microgrids. This paper focuses on the secondary frequency control of the VSM-based MGC.

Modeling of microgrids is the basis for secondary control law design. Comprehensive linearized model of microgrids was proposed in [6]. But the linearized model can only describes the system dynamics near a certain operating point, and the high order of [6] makes the tuning of control parameters complicated. Some literature studied both frequency and voltage restorations in the secondary control, but most of them neglected dynamics of LC filters, local loads and distribution networks in the microgrid modeling [7], [8]. Some literature only considered active power-frequency (P-f) response model in the secondary frequency control, in which DGUs, ESUs and

even the whole microgrid were simplified as first-order inertial links with certain time constants [9], [10]. But the P-f response model is not applicable for low voltage (LV) microgrids whose frequency is coupled with both active and reactive power. Simplified microgird models reduce the computational burden of tuning control parameters, but inaccurate modeling naturally deteriorates performance of the synthesized controllers. Model order reduction [11] and dynamic equivalencing [12] are commonly used techniques to reduce the microgrid models. Generally, dynamic equivalencing is preferred as it retains equivalent physical meanings in the reduced model. Note that the VSM-based microgrid can be equivalent to a modified synchronous generator (SG) model due to the inertial merits of the VSM [13].

Generally, centralized, decentralized and distributed control are three common approaches in the secondary level of the hierarchical control structure. The centralized approach requires a central controller in the MGC to coordinate each microgrid restoring the whole system frequency [14]. However, any failure in the central controller or communication inevitably affects the frequency restoration of the whole MGC [15]. The decentralized approach is based on local signals without relying on the central controller and communication [16], [17]. But the adjustment time would be prolonged with decentralized approaches [15]. Besides, most decentralized approaches depend on precise modeling of the whole system so as to remedy the absence of communication [18]. The distributed approach mostly depends on the multi-agent system and requires sparse communication between neighboring agents, which performs high intelligence, strong scalability and high redundancy [15], [19]. Because the tertiary control of each microgrid is mostly implemented via the centralized approach by the microgrid central controller (MGCC), the fully distributed approach requires upgrading of each microgrid so as to form the multi-agent system.

Due to the advantage of disturbance attenuation, robust control theory has been applied in microgrids operation. In [9], the H_∞ robust control and μ-synthesis techniques were used to develop the centralized secondary frequency control for microgrids, and the μ-synthesis approach showed better performance than the H_∞ method due to considering uncertain parameters as structured uncertainties. But the order of the synthesized controller was not smaller than that of the controlled system. In [20], the H_∞ robust theorem was used in tuning optimal parameters of the extended VSM to improve the robustness and stability of the microgrid frequency. But similar to [9], only the P-f response was considered in the microgrid modeling. In [21], the decentralized mixed H_2/H_∞ control was used to derive a 2nd-order controller embedded in the droop control scheme of each DGU, so as to improve the voltage reference tracking and disturbance rejection. But the uncertainties of modeling errors caused by the variations of inputs and disturbances were not considered in the linearized microgrid model.

Considering the limitations of above-mentioned works, this paper proposes a robust secondary frequency control design method for the VSM-based LV MGC. The equivalent SG (EqSG) model and unstructured uncertainties are used to construct the MGC model. To exploit the existing centralized control structure within each microgrid and the flexibility of the distributed control structure, this paper proposes a distributed-centralized hybrid control structure. Instead of using the conventional H_∞ robust or μ-synthesis methodology, the structured μ-synthesis is used to determine parameters of each secondary frequency controller. To reduce the consumption of communication bandwidth, the event-triggered mechanism [22] is introduced in the transmission of frequency deviations. The major contributions of this paper are as follows:

1) In the modeling process, each microgrid is equivalenced to the EqSG model so as to reduce the MGC model and the complexity of synthesizing secondary frequency controllers and event-triggering parameters. Different from [9], modeling errors caused by equivalent modeling, model linearization and variations of inputs and disturbances are considered as unstructured uncertainties in the MGC model.

2) The proposed secondary frequency control strategy adopts distributed-centralized hybrid control structure. The secondary frequency controller located in each MGCC receives frequency deviations from adjacent microgrids based on low bandwidth sparse communication through distributed approach. The frequency restoration is realized by correcting active and reactive power references provided by each MGCC, which is suitable for LV microgrids. Within each microgrid, the power corrections are assigned to each DGU, ESU and CL through centralized approach to realize reasonable power sharing.

3) To address the disturbances of RESs and local loads as well as uncertainties of modeling errors, the structured μ-synthesis based on D-K iteration is applied in tuning secondary frequency controller with predefined structure to realize H_∞ robust performance. Besides, the event-triggering parameters are determined through a Lyapunov function so as to guarantee H_∞ robust stability of the MGC with the proposed secondary frequency control.

The remainder of this paper is organized as follows: The equivalent MGC modeling considering unstructured uncertainties is elaborated in Section II. The distributed-centralized control structure and structured μ-synthesis of the proposed secondary frequency controller are illustrated in Section III. In Section IV, the event-triggered mechanism is integrated in the MGC model, and the determination of triggering parameters is introduced. The effectiveness and robustness of the proposed secondary frequency control strategy are examined in Section V. Section VI discusses the extension of the proposed method. Section VII concludes this paper.

II. Equivalent Model of the Microgrid Cluster

The basic structure of MGC is illustrated as Fig. 1(a), in which each microgrid consists of SGs, DGUs, ESUs, CLs and uncontrollable loads. To improve total inertia of the MGC system, DGUs, ESUs and CLs all adopt the VSM control. For simple expression, any unit that adopts the VSM control is

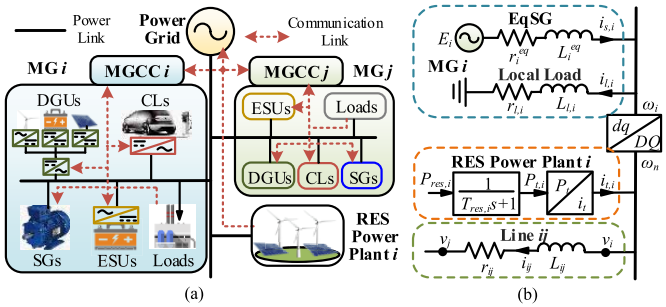

Fig. 1. Modeling of the MGC: (a) Structure of the MGC. (b) Illustration of equivalent modeling for the MGC.

referred to as a VSM. The intermittent RES is considered and presented as distributed RES power plants in the MGC.

A. Equivalent Model of Each Microgrid

For the VSM-based microgrid, its slow dynamics are mainly dominated by SGs and VSM control loops. For modeling simplification and not losing generality, all the VSMs and SGs in each microgrid are equivalenced to the EqSG model as (1) through gray-box system identification.

$$\begin{cases} J_i^{eq}\dot{\omega}_i = (P_{m,i} - P_{e,i})/\omega_n - D_{p,i}^{eq}(\omega_i - \omega_n), \\ K_i^{eq}\dot{E}_i = Q_{m,i} - Q_{e,i} - D_{q,i}^{eq}(U_{x,i} - U_{r,i}), \\ L_i^{eq}\dot{i}_{sd,i} = E_i - v_{d,i} - r_i^{eq} i_{sd,i} + \omega_i L_i^{eq} i_{sq,i}, \\ L_i^{eq}\dot{i}_{sq,i} = -v_{q,i} - r_i^{eq} i_{sq,i} - \omega_i L_i^{eq} i_{sd,i}, \\ P_{e,i} = 1.5(v_{d,i} i_{sd,i} + v_{q,i} i_{sq,i}), \\ Q_{e,i} = 1.5(v_{q,i} i_{sd,i} - v_{d,i} i_{sq,i}), \\ U_{x,i} = (1 - r_{x,i}^{eq})E_i + r_{x,i}^{eq}\sqrt{v_{d,i}^2 + v_{q,i}^2}, \end{cases} \tag{1}$$

where the subscript i denotes the ith microgrid, the subscript d or q denotes direct or quadratic component of the local rotational reference frame with angular frequency ω_i, $(v_{d,i}, v_{q,i})$ are voltages at the point of common coupling, $(i_{sd,i}, i_{sq,i})$ are output currents of the EqSG, E_i is the virtual internal electromotive force, $U_{x,i}$ is the equivalent internal voltage, $P_{m,i}$ and $Q_{m,i}$ are the sum of active and reactive power references of VSMs and SGs, respectively; $P_{e,i}$ and $Q_{e,i}$ are the sum of output active and reactive power of VSMs and SGs, respectively; variables with the superscript eq denote equivalent parameters derived from the gray-box system identification. To avoid over explanation, the detailed procedure of deriving the EqSG model can be referred to [13].

In each microgrid, uncontrollable loads are aggregated into a local load according to the sum of their power, which is modeled as the combination of resistance $r_{l,i}$ and inductance $L_{l,i}$ as:

$$\begin{cases} \dot{i}_{ld,i} = \left(v_{d,i} - r_{l,i} i_{ld,i}\right)/L_{l,i} + \omega_i i_{lq,i}, \\ \dot{i}_{lq,i} = \left(v_{q,i} - r_{l,i} i_{lq,i}\right)/L_{l,i} - \omega_i i_{ld,i}, \\ i_{d,i} = i_{sd,i} - i_{ld,i}, \\ i_{q,i} = i_{sq,i} - i_{lq,i}, \end{cases} \tag{2}$$

where $(i_{ld,i}, i_{lq,i})$ are currents of the local load, $(i_{d,i}, i_{q,i})$ are output currents of the ith microgrid. Thus, the equivalent model of each microgrid is obtained and illustrated as Fig. 1(b). Based on differential algebraic equations (DAEs) (1) and (2), linearized model of each microgrid can be obtained and expressed in the state-space format:

$$\begin{cases} \Delta\dot{x}_i = A_i\Delta x_i + B_i\Delta y_{Ni} + B_i^w\Delta w_i + B_i^u\Delta u_i \\ \Delta y_i = C_i\Delta x_i \end{cases}$$
$$\Delta x_i = \left[\Delta\omega_i, \Delta E_i, \Delta i_{sd,i}, \Delta i_{sq,i}, \Delta i_{ld,i}, \Delta i_{lq,i}\right]^T,$$
$$\Delta y_{Ni} = \left[\Delta v_{d,i}, \Delta v_{q,i}\right]^T, \ \Delta y_i = \left[\Delta\omega_i, \Delta i_{d,i}, \Delta i_{q,i}\right]^T,$$
$$\Delta w_i = \left[\Delta r_{l,i}, \Delta L_{l,i}\right]^T, \ u_i = \left[\Delta P_{m,i}, \Delta Q_{m,i}\right]^T, \tag{3}$$

where A_i, B_i, C_i, B_i^w and B_i^u are state-space matrices obtained according to the nominal operating condition, Δ denotes small perturbation; Δx_i, Δy_i and Δw_i are states, outputs and disturbances of the ith equivalent microgrid, respectively; Δy_{Ni} contains variables from the distribution network model to be introduced later; Δu_i contains power corrections from the robust secondary frequency controller.

B. Remainder of the MGC

The RES power plant is considered as the disturbed power source expressed by (4), shown as Fig. 1(b).

$$\begin{cases} T_{res,i}\dot{P}_{t,i} = P_{res,i} - P_{t,i}, \\ i_{tD,i} = \dfrac{2P_{t,i}\cos\left(\arctan\left(v_{Q,i}/v_{D,i}\right)\right)}{3\sqrt{{v_{D,i}}^2 + {v_{Q,i}}^2}}, \\ i_{tQ,i} = \dfrac{2P_{t,i}\sin\left(\arctan\left(v_{Q,i}/v_{D,i}\right)\right)}{3\sqrt{{v_{D,i}}^2 + {v_{Q,i}}^2}}, \end{cases} \tag{4}$$

where the subscript D or Q denotes direct or quadratic component of the common rotational reference frame with nominal angular frequency ω_n, $(i_{tD,i}, i_{tQ,i})$ are injection currents to the ith microgrid, $P_{res,i}$, $P_{t,i}$ and $T_{res,i}$ denotes input, output power and time constant of the ith RES power plant, respectively.

Modeling of the distribution line is referred to [6], shown as Fig. 1(b). Note that the reference frame transformation introduces δ_i the integral of frequency deviation by $\dot{\delta}_i = \omega_i - \omega_n$, which is to be used in the secondary frequency controller. Combining (4), the rest part of the MGC can be expressed as:

$$\begin{cases} \Delta\dot{x}_N = A_N\Delta x_N + B_N\Delta y_\Sigma + B_N^w\Delta w_N \\ \Delta y_N = C_N\Delta x_N + D_N\Delta y_\Sigma + D_N^w\Delta w_N \end{cases}$$
$$\Delta\Lambda = [\Delta\Lambda_1, \Delta\Lambda_2, \ldots, \Delta\Lambda_n]^T, \ \Lambda \text{ means } x_N, w_N \text{ or } y_N,$$
$$\Delta x_{Ni} = \left[\Delta\delta_i, \Delta i_{D,ij}, \Delta i_{Q,ij}, \Delta P_{t,i}\right]^T, \Delta w_{Ni} = \Delta P_{res,i},$$
$$\Delta y_\Sigma = \left[\Delta y_1, \Delta y_2, \ldots, \Delta y_n\right]^T, \tag{5}$$

where A_N, B_N, B_N^w, C_N, D_N and D_N^w are state-space matrices obtained according to the nominal operating condition; $(i_{D,ij}, i_{Q,ij})$ are currents of distribution lines, the subscript ij indicates connection between the ith and the jth microgrid, Δx_N and $\Delta y_{N\Sigma}$ are states and outputs of the distribution network, respectively; Δw_N denotes disturbances from the RES power plants, Δy_Σ contains variables from each microgrid, the subscript n denotes the number of microgrids in the MGC.

C. Complete MGC Model

Combining (3) and (5), the linearized nominal MGC model can be obtained as (6), as shown at the bottom of the next page, (Δ is omitted for simple expression), where $\mathbf{0}$ denotes the zero matrix with proper dimension.

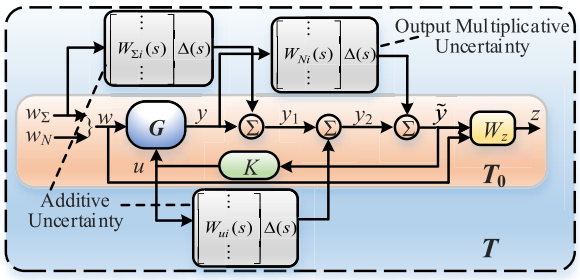

Fig. 2. Complete MGC model with unstructured uncertainties.

As mentioned in [13], the EqSG model inevitably loses high-frequency dynamics to some degree. Besides, the linearized model (6) fails to accurately describe dynamics of the MGC when variations of disturbances or inputs make the system deviate from the nominal condition. For robust control design, unmodeled dynamics and modeling errors, i.e., unstructured uncertainties, are often addressed by introducing perturbation blocks $W(s)\Delta(s)$ through additive or multiplicative approaches [9], [23], where $\Delta(s)$ denotes uncertain dynamics with unit peak magnitude, $W(s)$ is a stable, minimum-phase shaping filter such that frequency response of $W(s)\Delta(s)$ covers the influence of unstructured uncertainties. For accurately modeling unstructured uncertainties, in this paper, if there are more indices in u, w_N or w_Σ than y, unstructured uncertainties caused by corresponding inputs are modeled in the additive approach. Otherwise, they are modeled in the output multiplicative approach. In order to reduce the conservativeness of unstructured uncertainties, shaping filters are designed as the single-input multi-output structure.

Thus, the complete MGC model is established as Fig. 2, where G denotes the linearized nominal MGC model (6), K denotes the robust secondary frequency controller to be designed, W_z denotes the weighting function used for normalizing disturbances and observed variables, $W_{u,i}(s)$, $W_{N,i}(s)$ and $W_{\Sigma,i}(s)$ are shaping filters obtained by fitting the upper bounds of frequency-domain response errors between the detailed MGC model and (6) under possible u, w_N and w_Σ, respectively; T_0 denotes the nominal closed-loop MGC model with weighting function, T denotes the complete MGC model considering unstructured uncertainties.

III. Design of the Robust Secondary Frequency Controller

A. Distributed-Centralized Control Structure

The proposed robust secondary frequency control strategy is installed in each MGCC to construct the distributed-centralized control structure, as illustrated in Fig. 3(a). The control

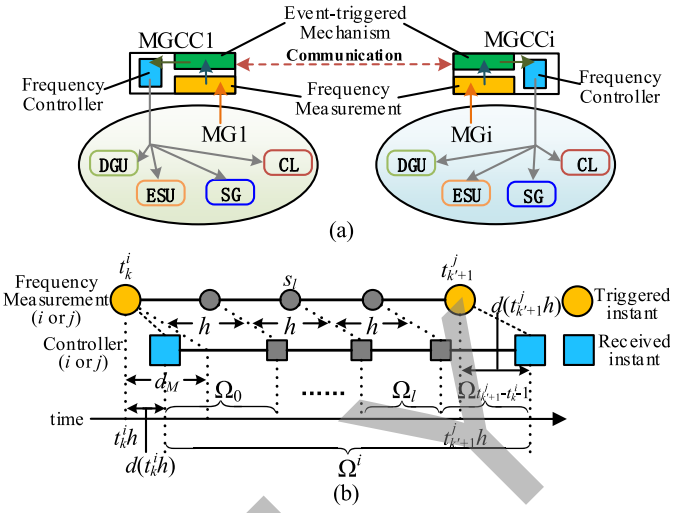

Fig. 3. Illustration of robust secondary frequency control strategy: (a) Distributed-centralized control structure; (b) Time sequence in Ω^i.

structure among MGCCs is implemented in the distributed approach. The MGCC of each microgrid calculates local frequency deviation and receives frequency deviations from neighboring MGCCs. The robust secondary frequency controller generates the power correction signals ($\Delta P_{m,i}$, $\Delta Q_{m,i}$), and then the power corrections are dispatched by the MGCC to local VSMs in the centralized approach according to (7) such that realize frequency restoration of the whole MGC system and proper power sharing within each microgrid. The distributed-centralized control structure exploits the existing centralized control structure within each microgrid as well as advantages of the distributed control structure.

$$(\Delta P_i, \Delta Q_i) = \frac{S_i}{\sum_{i=1}^{n_g} S_i}\left(\Delta P_{m,i}, \Delta Q_{m,i}\right), \tag{7}$$

where $(\Delta P_i, \Delta Q_i)$ and S_i denote power corrections and rated power of the ith VSM, n_g is the number of local VSMs.

Before introducing the robust secondary frequency controller, the basic graph theory is explained, because parameters of the proposed controllers are related to the communication topology. The communication linkage among MGCCs can be described as an undirected graph $\mathcal{G} = \{\mathcal{V}, \mathcal{E}, \mathcal{W}\}$ (assumed to be connected) of order n, where $\mathcal{V} = \{v_1, v_2, \ldots, v_n\}$ and $\mathcal{E} \subseteq \mathcal{V} \times \mathcal{V}$ denote the set of nodes and edges with n indicating the number of microgrids, respectively. The set of neighbors of the ith MGCC is $\mathcal{N}_i = \{j \in \mathcal{V} | (i,j) \in \mathcal{E}\}$. The adjacency matrix of $\mathcal{G}$ is $\mathcal{W} = (w_{ij})_{n\times n}$ with $w_{ii} = 0$, $w_{ij} = 1$ if $(i,j) \subseteq \mathcal{E}$, otherwise $w_{ij} = 0$. The degree matrix of $\mathcal{G}$ is $\mathcal{D} = diag(\bar{w}_1, \ldots, \bar{w}_i, \ldots, \bar{w}_n)$ with $\bar{w}_i = \sum_{j=1}^{n} w_{ij}$ denoting the number of neighbors for the ith MGCC.

$$\begin{cases} \dot{x} = Ax + B_1 w + B_2 u \\ \quad = \begin{bmatrix} \dot{x}_\Sigma \\ \dot{x}_N \end{bmatrix} = \left[\begin{array}{c|c} A_\Sigma + B_\Sigma D_N C_\Sigma & B_\Sigma C_N \\ \hline B_N C_\Sigma & A_N \end{array}\right] \begin{bmatrix} x_\Sigma \\ x_N \end{bmatrix} + \left[\begin{array}{c|c} B_\Sigma^w & B_\Sigma D_N^w \\ \hline \mathbf{0} & B_N^w \end{array}\right] \begin{bmatrix} w_\Sigma \\ w_N \end{bmatrix} + \begin{bmatrix} B_\Sigma^u \\ \mathbf{0} \end{bmatrix} \begin{bmatrix} u \\ \mathbf{0} \end{bmatrix} \\ y = [y_{K1}, y_{K2}, \ldots, y_{Kn}]^T = Cx, y_{Ki} = [\omega_i, \delta_i]^T \end{cases}$$
$$\Lambda_\Sigma = [\Lambda_1, \Lambda_i, \ldots, \Lambda_n]^T, \Lambda \text{ means } x \text{ or } w; \quad \mathrm{X}_\Sigma = diag(\mathrm{X}_1, \mathrm{X}_2, \ldots, \mathrm{X}_n), \mathrm{X} \text{ means } A, B, B^w \text{ or } B^u \tag{6}$$

Algorithm 1 D-K Iteration for Structured μ-Synthesis

1. *Initial K step:* Uses H_∞ synthesis to find a feasible controller K that $\min\|T_0\|_\infty$.
2. *D step:* Computes the upper bound $\bar{\mu}$ of the structured singular value for T, i.e., $\bar{\mu} = \max_i \mu_i$ with $\mu_i = \inf_{\omega_i} \|T(j\omega_i)\|_\infty$. Finds an invertible function $D(s)$ that fits $\left\|D(j\omega_i)T_0(j\omega_i)D^{-1}(j\omega_i)\right\|_\infty = \mu_i$.
3. *K step:* Uses H_∞ synthesis to find a controller K that $\min\left\|D(s)T_0D^{-1}(s)\right\|_\infty$.
4. Return to Step 2 until $\bar{\mu}$ stops improving at γ or is less than a prescribed H_∞ norm bound γ.

B. Structured μ-Synthesis Robust Controller

Different from [9] using traditional H_∞/μ-synthesis, whose derived controller order is fixedly equal to the system model order and control structure is implemented in the centralized approach, the structured μ-synthesis can realize H_∞ robust performance for the system considering unstructured uncertainties with predefined controller structure. In this paper, the secondary frequency controller located in each MGCC is defined as:

$$u_i = K_i\begin{bmatrix}\left(\sum_{j\in N_i}\left(\Delta\omega_j\right) + \Delta\omega_i\right)/(\bar{w}_i+1)\\ \Delta\delta_i\end{bmatrix}, \tag{8}$$

where $K_i \in \boldsymbol{R}^{2\times 2}$ is the ith secondary frequency controller, $\Delta\omega_i$ and $\Delta\delta_i$ denote frequency deviation and its integral of the ith microgrid, respectively. It can be seen that the proposed controller uses the structure of PI control. The proportional part is based on the average of local and neighboring frequency deviations so as to coordinate the frequency regulation among microgrids. The integral part uses the integral of the local frequency deviation so that avoid the adverse effects of communication failure. The control action signal u_i is active and reactive power corrections ($\Delta P_{m,i}$, $\Delta Q_{m,i}$) as expressed in (3), which is suitable for the frequency restoration of LV and MV microgrids.

The aggregated secondary frequency control law of the MGC system is described as:

$$u = Ky, \quad K = \left[K_1A_{d,1}, \ldots, K_iA_{d,i}, \ldots, K_nA_{d,n}\right]^T, \tag{9}$$

where $A_{d,i}$ denotes the weighted adjacency matrix providing proper inputs for K_i. According to (6) and (8), $A_{d,i}$ can be expressed as $A_{d,i} = A_d(2i-1{:}2i, :)$ with

$$A_d = (\mathcal{D}+I_n)^{-1}(\mathcal{W}+I_n)^T \otimes \begin{bmatrix}1 & 0\\ 0 & 0\end{bmatrix} + I_n \otimes \begin{bmatrix}0 & 0\\ 0 & 1\end{bmatrix},$$

where I_n denotes the identity matrix of size n.

To improve robustness of the secondary frequency controller against disturbances and variations of operation conditions, the structured μ-synthesis based on D-K iteration is used to determine parameters of the secondary frequency controller. The main procedure of tuning K is shown as Algorithm 1.

The robust performance of the closed loop MGC system T is measured by γ as the peak gain (under any frequency) of T remains below γ for the modeled uncertainties up to $1/\gamma$ (in normalized units). Thus, the robust stability is guaranteed if $\gamma < 1$. Note that the proper selection of the weighting function W_z in T_0 and T is crucial for deriving appropriate control parameters such that preserve satisfactory robust performance and stability.

IV. Design of Event-Triggering H_∞ Robust Secondary Frequency Control

A. Event-Triggered Mechanism

It is assumed that the local frequency is sampled with a constant period h and the sampling instants are synchronized among MGCCs based on the global position system. Thus the set of sampling instants of frequency deviations can be denoted as $\mathbf{S} = \{0, 1h, 2h, \ldots\}$. To reduce unnecessary sampling transmitting in the communication network, the event-triggered mechanism is introduced. The transmitting instant of the ith MGCC is determined as:

$$t_{k+1}^i h = t_k^i h + \min_{l\in N}\big\{lh \big| y_{ei}^T(s_l h)\Phi_i y_{ei}(s_l h) > \sigma_i y_{Ki}^T\big(t_k^i h\big)\Phi_i y_{Ki}\big(t_k^i h\big)\big\}, \tag{10}$$

where $t_k^i h \in \mathbf{S}$ with subscript $k = (1, 2, 3\cdots)$ denoting the kth transmitting instant and superscript i denoting the ith MGCC, $s_l = t_k^i + l$ with $l = (1, 2, \ldots, t_{k+1}^i - t_k^i)$, $y_{ei}(s_l h) = y_{Ki}(s_l h) - y_{Ki}(t_k^i h)$, $\Phi_i \in \boldsymbol{R}^{2\times 2}$ is a weighted triggering matrix of the ith MGCC to be designed, $\sigma_i > 0$ is a predetermined parameter.

The communication delay between MGCCs is considered as $d(t) \in [0, d_M]$ with $\dot{d}$ denoting its rate of change, where d_M is the upper bound of communication delay ($d_M \le h$ is assumed in this paper). Note that the communication delay within the microgrid is not considered since the scale of the LV microgrid is generally small. Consider the time interval of two adjacent instants that any MGCC receives new frequency information as $\Omega^i = [t_k^i h + d(t_k^i h), t_{k'+1}^j h + d(t_{k'+1}^j h))$, where $t_{k'+1}^j$ denotes the upcoming transmitting instant from the jth MGCC (j can be i). Thus, the ith secondary frequency control law (8) can be expressed as:

$$u_i(t) = K_i\begin{bmatrix}\frac{\sum_{j\in N_i}\left(\Delta\omega_j(t_{k'}^j h)\right)+\Delta\omega_i(t_k^i h)}{(\bar{w}_i+1)}\\ \Delta\delta_i\big(t_k^i h\big)\end{bmatrix}, \ t \in \Omega^i,$$

which indicates that the ith secondary frequency controller is updated when it receives new frequency information from whether its local event-triggered mechanism or neighboring MGCCs. Then the aggregated secondary frequency control law (9) can be rewritten as:

$$u(t) = K\hat{y}\big(t_k^i h\big) = K\big[y(s_l h) - C\zeta(s_l h)\big], \ t \in \Omega^i,$$

where $\hat{y}(t_k^i h)$ denotes the actual inputs of (9) with $t \in \Omega^i$, $C\zeta(s_l h)$ denotes the error between $y(s_l h)$ and $\hat{y}(t_k^i h)$.

The time interval Ω^i can be divided into h-based subsets $\cup_{l=0}^{t_{k'+1}^i - t_k^i}\Omega_l$ as illustrated in Fig. 3(b). Thus, for $t \in \Omega_l$, the actual inputs of (9) can be expressed as:

$$\hat{y}(t) = C\big[x\big(t - d\big(t_k^i h\big)\big) - \zeta(s_l h)\big], \ t \in \Omega_l. \tag{11}$$

The MGC model (6) with secondary frequency controller considering event-triggered mechanism can be formulated as:

$$\begin{cases} \dot{x}(t) = Ax(t) + B_1 w(t) + B_2 KCx\big[t - d\big(t_k^i h\big)\big] \\ \qquad - B_2 KC\zeta(s_l h) \\ y(t) = Cx(t), t \in \Omega_l. \end{cases} \tag{12}$$

B. Design of Event-Triggering Parameter

According to (6), (10) and (11), the distributed event-triggered mechanism of each MGCC can be summed and expressed in the aggregated form as:

$$\Big[F\tilde{C}\zeta(s_l h)\Big]^T \Phi F\tilde{C}\zeta(s_l h) > \Big[F_\sigma \tilde{C}x\big(t_k^i h\big)\Big]^T \Phi F_\sigma \tilde{C}x\big(t_k^i h\big), \tag{13}$$

where $F = diag(F_1, F_2, \ldots, F_n)$, $F_i = I_n(i,:) \otimes I_2$, $\Phi = diag(\Phi_1, \Phi_2, \ldots, \Phi_n)$, $F_\sigma = diag(\sqrt{\sigma_1}F_1, \sqrt{\sigma_2}F_2, \ldots, \sqrt{\sigma_n}F_n)$, $\tilde{C} = 1_n \otimes C$ with 1_n denoting the vector of size n whose entries are ones. To ensure H_∞ robust stability of the whole MGC secondary frequency control under the event-triggered mechanism, the event-triggering parameter Φ_i of each MGCC is determined according to the following linear matrix inequalities (LMIs).

Theorem 1: For given constant $\sigma_i > 0$, $d_M > 0$, $\dot{d}$, if there exists positive definite matrices P, Q_1, Q_2, R, Φ, appropriate dimensions X_1, X_2, X_3, X_4, and the following LMIs hold, the studied MGC model (12) is asymptotically stable with the H_∞ norm bound γ.

$$\Xi < 0, \tag{14}$$

$$\hat{R} = \begin{bmatrix} \tilde{R} & * \\ X & 3\tilde{R} \end{bmatrix} > 0, \tag{15}$$

where

$$\begin{aligned} \Xi = {} & e_1^T \nu_1 e_1 - \big(1 - \dot{d}\big)e_3^T Q_1 e_3 - e_4^T Q_2 e_4 - \gamma^2 e_5^T e_5 \\ & + e_1^T C^T C e_1 + \Big[F_\sigma \tilde{C}e_1\Big]^T \Phi F_\sigma \tilde{C}e_1 - \Big[F\tilde{C}e_2\Big]^T \Phi F\tilde{C}e_2 \\ & + 2\eta^T P e_1 + d_M \eta^T R \eta - \chi^T \hat{R}\chi, \end{aligned}$$

$$\nu_1 = Q_1 + Q_2,\ e_j = \Big[\underbrace{0 \cdots 0}_{j-1}, 1, \underbrace{0 \cdots 0}_{7-j}\Big]^T, (j = 1, \ldots, 7),$$

$$\eta = [Ae_1 - B_2 KCe_2 + B_2 KCe_3 + B_1 e_5],\ \chi = \begin{bmatrix} \chi_1 \\ \chi_2 \end{bmatrix},$$

$$\chi_1 = \begin{bmatrix} e_1 - e_3 \\ e_1 + e_3 - 2e_6 \end{bmatrix},\ \chi_2 = \begin{bmatrix} e_3 - e_4 \\ e_3 + e_4 - 2e_7 \end{bmatrix},$$

$$\tilde{R} = \begin{bmatrix} R & * \\ 0 & 3R \end{bmatrix},\ X = \begin{bmatrix} X_1 & X_2 \\ X_3 & X_4 \end{bmatrix}.$$

Proof: Construct the Lyapunov function as the following:

$$\begin{aligned} V(x(t)) = {} & x^T(t)Px(t) + \int_{t-d(t_k^i h)}^{t} x^T(s)Q_1 x(s)ds \\ & + \int_{t-d_M}^{t} x^T(s)Q_2 x(s)ds \\ & + d_M \int_{-d_M}^{0} \int_{t+\alpha}^{t} \dot{x}^T(s)R\dot{x}(s)dsd\alpha \end{aligned}$$

Calculating the derivative of $V(x(t))$ along the trajectory of the studied model (12) yields:

$$\begin{aligned} \dot{V}(x(t)) = {} & x^T(t)\nu_1 x(t) - \big(1 - \dot{d}\big)x^T\big(t - d\big(t_k^i h\big)\big)Q_1 x\big(t - d\big(t_k^i h\big)\big) \\ & - x^T(t - d_M)Q_2 x(t - d_M) + 2\dot{x}^T(t)Px(t) \\ & + d_M \dot{x}^T(t)R\dot{x}(t) - d_M \int_{t-d_M}^{t} \dot{x}^T(s)R\dot{x}(s)ds \end{aligned}$$

By applying Wirtinger inequality, the following inequality can be obtained:

$$\begin{aligned} -d_M \int_{t-d_M}^{t} \dot{x}^T(s)R\dot{x}(s)ds = {} & -d_M \int_{t-d\left(t_k^i h\right)}^{t} \dot{x}^T(s)R\dot{x}(s)ds \\ & - d_M \int_{t-d_M}^{t-d\left(t_k^i h\right)} \dot{x}^T(s)R\dot{x}(s)ds \\ \le {} & -W^T \hat{R} W \end{aligned}$$

where $\hat{R}$ is the matrix satisfying the condition (15), $W = [W_1,\ W_2]^T$ with

$$W_1 = \begin{bmatrix} x(t) - x\big(t - d\big(t_k^i h\big)\big) \\ x(t) + x\big(t - d\big(t_k^i h\big)\big) - \frac{2}{d\left(t_k^i h\right)} \int_{t-d\left(t_k^i h\right)}^{t} x(s)ds \end{bmatrix},$$

$$W_2 = \begin{bmatrix} x\big(t - d\big(t_k^i h\big)\big) - x(t - d_M) \\ x\big(t - d\big(t_k^i h\big)\big) + x(t - d_M) - \frac{2}{d_M - d\left(t_k^i h\right)} \int_{t-d_M}^{t-d\left(t_k^i h\right)} x(s)ds \end{bmatrix}.$$

Considering the triggering condition (13), the following inequality can be obtained:

$$\dot{V}(x(t)) < \xi^T(t)\Xi\xi(t) - y^T(t)y(t) + \gamma^2 \omega^T(t)\omega(t),$$

where $\xi(t)$ is the augmented vector as:

$$\begin{aligned} \xi(t) = \Bigg[& x(t),\ \zeta(s_l h),\ x\big(t - d\big(t_k^i h\big)\big),\ x(t - d_M),\ w(t), \\ & \times \frac{1}{d\big(t_k^i h\big)} \int_{t-d\left(t_k^i h\right)}^{t} x(s)ds, \\ & \times \frac{1}{d\big(t_k^i h\big) - d_M} \int_{t-d_M}^{t-d\left(t_k^i h\right)} x(s)ds \Bigg]^T. \end{aligned}$$

If the condition (14) is satisfied, under the condition $\omega(t) = 0$, there exists a sufficiently small scalar $\varepsilon > 0$ such that $\dot{V}(x(t)) < -\varepsilon\|\xi(t)\|^2 < 0$.

Considering the cost function $J = \int_0^\infty y^T(t)y(t) - \gamma^2 w^T(t)w(t)dt$ with the disturbance $\omega(t) \in L_2[0, \infty)$, the following inequality can be obtained:

$$V(x(\infty)) - V(x(0)) + J < 0.$$

Under the zero initial condition $V(x(0)) = 0$ and $\lim_{t\to\infty} V(x(t)) \ge 0$, the cost function $J < 0$, i.e., $\|y(t)\| \le \gamma\|\omega(t)\|$. Thus, the MGC model (13) is asymptotically stable with the H_∞ robust performance γ. ■

V. Case Study

The effectiveness of the proposed robust secondary frequency control design method is verified in a MGC system composed by parallel connection of four CIGRÉ benchmark LV microgrids [24], where DGUs and ESUs in each microgrid all adopt the VSM control. The physical topology and communication connection of the studied MGC are illustrated in Fig. 4. For generality and simplicity, the disturbances of local loads are intensively performed at Load 5 of each microgrid. At the initial state, output power of the RES plant is 25kW and frequency of the whole system is 50Hz.

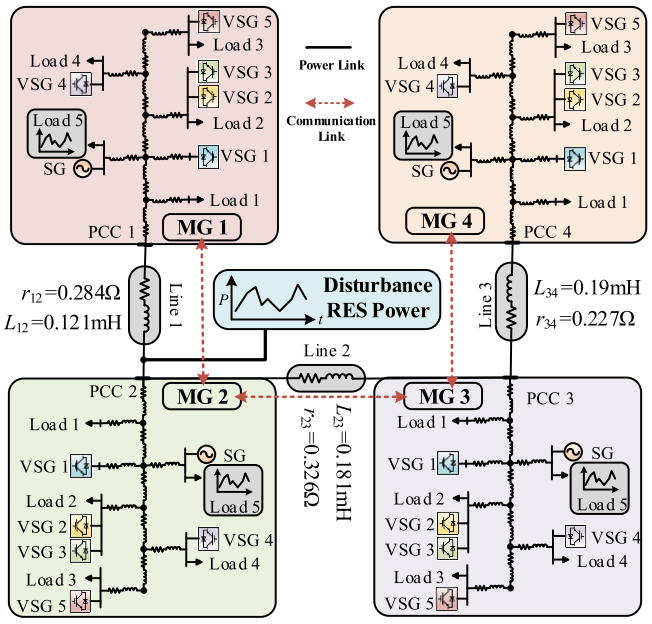

Fig. 4. Physical topology and communication connection of the studied MGC system.

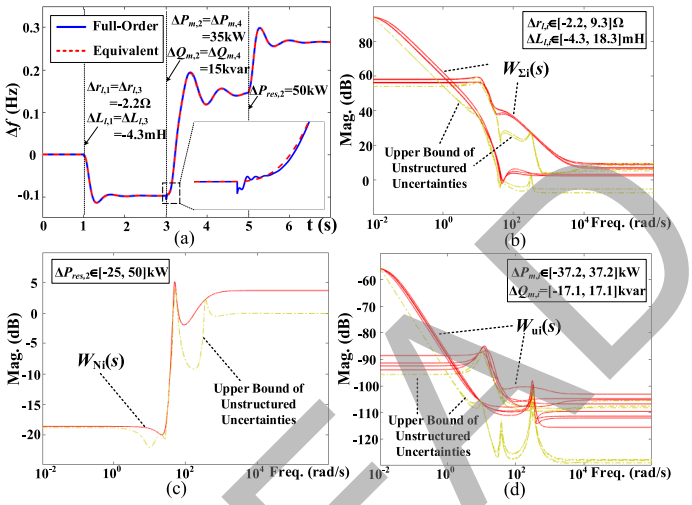

Fig. 5. Equivalent modeling of the studied MGC with unstructured uncertainties: (a) comparison between full-order and equivalent nominal MGC models, (b) shaping filters for local loads variations, (c) shaping filter for RES plant power variations, and (d) shaping filters for power instructions variations.

A. Equivalent Modeling With Unstructured Uncertainties

The full-order MGC model is obtained according to [6] with the order of 467, which is computationally prohibitive to be used in synthesizing secondary frequency controllers and event-triggering parameters. After the gray-box system identification-based dynamic equivalencing, the EqSG model of each microgrid is obtained with equivalent parameters as shown in the Appendix. Then the equivalent nominal MGC model is constructed according to Section II with the order of 35.

The comparison of dynamical responses between full-order and equivalent MGC models is demonstrated in Fig. 5(a). At $t = 1, 3, 5s$, the variations of local loads, power instructions and RES plant power are applied. It can be observed

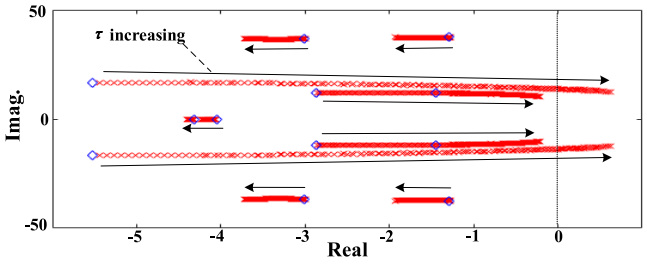

Fig. 6. Eigenvalue spectrum computed with τ varying from 0 to 0.12s.

that the equivalent model reflects dynamics of the full-order model with good accuracy, even though the equivalent model inevitably loses high-frequency dynamics to some degree.

To model unstructured uncertainties, frequency responses of the full-order MGC model under various operating conditions are analyzed, and upper bounds of frequency response errors with respect to the equivalent nominal MGC model are abstracted separately for each input channel. Using MATLAB/Control System Toolbox, the shaping filters are determined by fitting upper bounds of the frequency response errors with 3rd-order, as shown in Figs. 5(b)–(d). It can be observed that each shaping filter covers corresponding unstructured uncertainty.

B. Robust Secondary Frequency Control Design

To obtain required H_∞ robust performance, a proper design of weighting functions for the studied MGC model is:

$$W_z = \left[W_{z,l}(s) \quad W_{z,res}(s) \quad W_{z,y}(s) \right]^T,$$

where $W_{z,l}(s) = I_4 \otimes diag(0.081, \ 41.67)\dfrac{315.7}{s+31.57}$ is used for normalizing local loads disturbances, $W_{z,res} = \dfrac{12.62}{s+6.31}$ normalizes RES plant power disturbances, $W_{z,y} = 0.3183 I_8 \dfrac{0.1s+62.8}{s+6.28}$ is used for normalizing outputs.

Based on the structured μ-synthesis method elaborated in Algorithm 1, parameters of the proposed secondary frequency controllers are obtained using MATLAB/Robust Control Toolbox as: $K_1 = [-1.8007e4, -9.3166e4; 1.5165e4, 1.9206]$, $K_2 = [-8.4310e3, -1.4736e5; 2.9599e4, -2.079]$, $K_3 = [-8.6450e3, -1.4730e5; 9.7123e3, -163.5]$, $K_4 = [-1.6702e4, -9,6175e4; 1.5164e4, 2.0794]$. The H_∞ robust performance level is $\gamma = 0.784$.

Using MATLAB/LMI Toolbox to solve LMIs in Theorem 1 with $\sigma_i = 0.1$, $d_M = 0.02$, $\dot{d} = 0.05$, triggering parameters for the studied MGC system is derived as: $\Phi_1 = [10.9510, 0; 0, 10.0002]$, $\Phi_2 = [12.3854, 0.0001; 0.0001, 10.0010]$, $\Phi_3 = [12.5893, 0.0001; 0.0001, 10.0010]$, $\Phi_4 = [11.1816, 0; 0, 10.0002]$.

C. Eigenvalue and Time Delay Analysis

Note that the studied system model (12) is a time-delay linear system, where $d(t)$ is the communication time-delay. To simplify the eigenvalue analysis, it is assumed that the communication time-delay $d(t)$ is a constant value (denoted as τ)

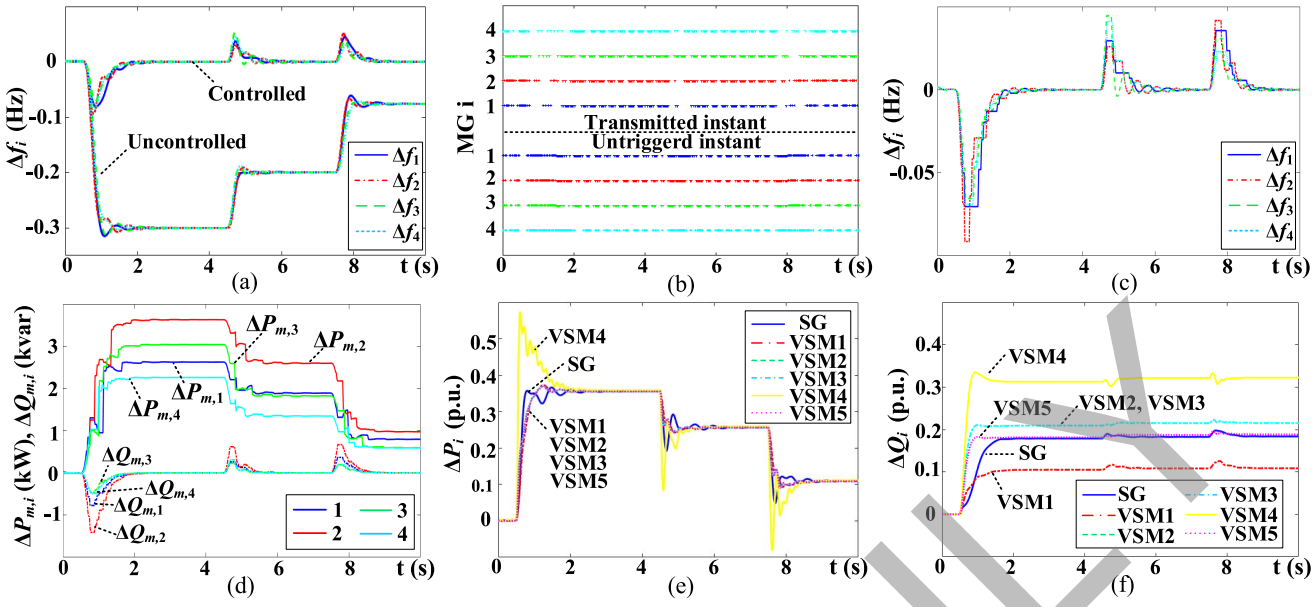

Fig. 7. Performance of the proposed secondary frequency control strategy: (a) frequency deviation of each microgrid, (b) transmitted and untriggered instants, (c) received frequency deviation of each controller, (d) output power correction instructions of each controller, (e) output active power deviations in MG1, and (f) output reactive power deviations in MG1.

within a sufficiently small time interval and throughout the whole communication network. According to the procedure provided in [25] (the number of Chebychev nodes is 20), the eigenvalue spectrum of the studied system with respect to varying τ from 0 to 0.12s is obtained as shown in Fig. 6, where the blue diamonds denote the eigenvalues without time-delay. It can be observed that the studied system is asymptotically stable when $\tau = 0$, and the stability of the system is degraded with the increasing of τ.

Then, the time-delay margin is analyzed. With the precondition that the studied system (12) is asymptotically stable for $\tau = 0$, the characteristic equation of (12) can be obtained as

$$D(j\omega, T) = \det\left(j\omega I - A - \tilde{A}\frac{1 - Tj\omega}{1 + Tj\omega}\right),$$

where $\tilde{A} = B_2KC$, ω and T are variables introduced by the Rekasius substitution. The time-delay margin τ_{max} can be calculated as $\tau_{\max} = \frac{2}{\omega_{\min}}\tan^{-1}(\omega_{\min}T_{\max})$, where ω_{min} is the minimal (infimum) of ω and T_{max} is the maximum (supremum) of T that subject to $|D(j\omega, T)| > 0$. To avoid over-explanation, the detailed procedure determining ω_{min} and T_{max} can be referred to [26]. Hence, the time-delay margin is determined as $\tau_{max} = 0.1152s$ with $\omega_{min} = 9.91$ and $T_{max} = 0.0648$. This value is tested in the following simulation verification.

D. Simulation Verification

The simulation model of the studied MGC system with the proposed secondary frequency control and event-triggered mechanism is built using MATLAB/SIMULINK. The sampling period of each frequency measurement is $h = 0.02$s and sampling instants are synchronized. The transmission time-delay of each communication link is generated according to the uniformly distributed random number such that $d(t) \in (0, d_M]$. Three typical disturbance scenarios are designed as follows:

1) *Disturbance 1:* Local load disturbances occur in MG1 and MG3 such that $\Delta r_{l,1} = \Delta r_{l,3} = -2.2\Omega$ and $\Delta L_{l,1} = \Delta L_{l,3} = -4.3$mH;

2) *Disturbance 2:* Local load disturbances occur in MG2 and MG4 such that $\Delta r_{l,2} = \Delta r_{l,4} = 9.3\Omega$ and $\Delta L_{l,2} = \Delta L_{l,4} = 18.3$mH;

3) *Disturbance 3:* RES plant power disturbance such that $\Delta P_{res,2} = 50$kW.

The simulation scenario proceeds as: At $t = 0.5$s, 4.5s and 7.5s, *Disturbance 1*, *Disturbance 2* and *Disturbance 3* are applied, respectively.

Performance of the proposed secondary frequency control is shown in Fig. 7. It can be observed in Fig. 7(a) that the proposed control strategy coordinates frequency restoration among microgrids with robustness against local loads and RES power disturbances. Fig. 7(b) exhibits transmitted and untriggered instants of each microgrid. Compared to period-triggered mechanism with transmission rate of 50Hz, the average transmission rate of the event-triggered mechanism in this MGC system is 23.5Hz, which avoids unnecessary transmission of 52.4% sampled data. Fig. 7(c) shows frequency deviations received by each MGCC, and Fig. 7(d) shows power corrections generated by each controller. It can be observed that the power corrections are not averagely shared among microgrids. This is because unstructured uncertainties are considered in the structured μ-synthesis procedure so that tuned control parameters in every MGCC are different. Uneven distribution of power corrections coordinates frequency restoration among microgrids as well as resists unstructured uncertainties. However, in each microgrid, the power corrections are shared among SGs and VSMs according to their nominal capacities, and proper active power sharing is realized as illustrated in Fig. 7(e). It can be seen from Fig. 7(f) that reactive power deviations are not equal to the power corrections and not

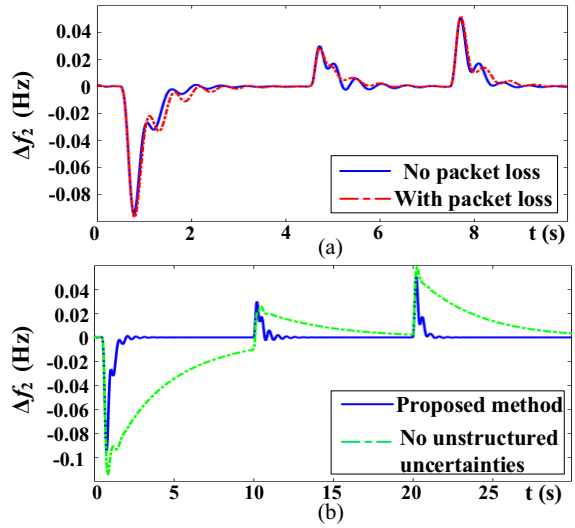

Fig. 8. Performance comparison: (a) robustness against packet loss, (b) comparison with controller designed without considering unstructured uncertainties.

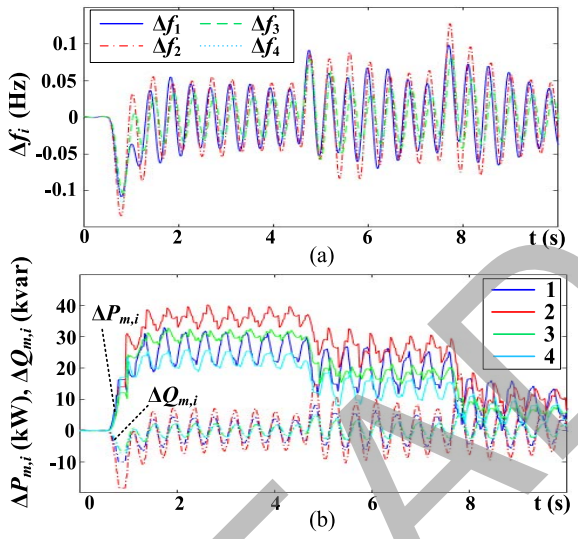

Fig. 9. Verification of time-delay margin: (a) frequency deviations under $\tau = 0.11s$, (b) power corrections under $\tau = 0.11s$.

properly shared. This is due to secondary voltage control is not considered in the studied MGC system, whereas active power deviations inevitably affect local voltage and output reactive powers of SGs and VSMs are related to the local voltage. Future study will aim at improving present control strategy to coordinate both frequency and voltage restorations.

To further test robustness of the proposed control strategy, the data drop-out (packet loss in all links) randomly occurs once in every 100ms. Corresponding performance comparison with no packet loss is shown in Fig. 8(a). It can be observed that frequency restoration only exhibits slightly delay under stochastic packet loss. This is because the event-triggered mechanism modeling includes possible packet loss as special cases [10]. Besides, the triggering parameters are derived realizing H_∞ robust stability, so that the proposed control strategy is robust to packet loss.

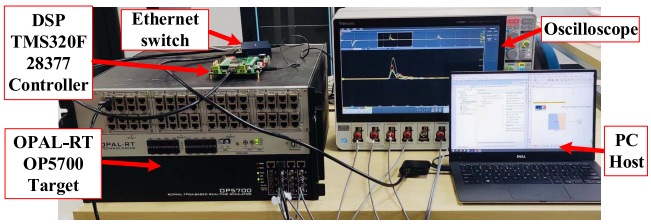

Fig. 10. Real-time experimental platform.

Fig. 8(b) compares frequency restoration performance with a centralized event-triggered PI control strategy, which forms the system model without considering unstructured uncertainties. It is clear that the control strategy designed without considering unstructured uncertainties exhibits slower restoration and larger overshoot, as its system modeling fails to cover different operating conditions and disturbances, hence deteriorating its robustness.

To verify the analyzed time-delay margin, the variable transmission time-delay of each communication link is set to a constant value $\tau = 0.11s$. It can be seen from Fig. 9 that the MGC system is in critical stable state. Hence, the analyzed time-delay margin $\tau_{max} = 0.1152s$ is verified. Because the scale of LV microgrids is relatively small and the communication delay is generally less than 20ms, the time-delay margin of the proposed control strategy can meet the practical requirements.

E. Real-Time Experimental Verification

The real-time experiment is implemented by using real-time simulator OPAL-RT OP5700 and digital signal processor (DSP) TMS320F28377, shown as Fig. 10. The studied MGC system (Fig. 4), event-triggered mechanism and variable communication delay with upper bound $d_M = 0.02s$ are contained in the SIMULINK model, which is executed in the OP5700 target in real time. The distributed secondary frequency controllers are realized in the DSP separately and independently. The frequency deviation of each microgrid (without communication delay) is converted and output as voltage signal through the analog I/O board in the OP5700 target, so that can be recorded by the digital oscilloscope. The power corrections generated by each frequency controller are recorded in the DSP and plotted with MATLAB. The basic test scenario is designed as: At $t = t_1$, t_3 and t_4, Disturbance 1, Disturbance 2 and Disturbance 3 are applied, respectively. To test the robustness of the proposed control strategy against communication or controller failure, the following scenarios are implemented in the real-time experiment platform.

Scenario 1 (Communication link 3 failure occurs at $t = t_2$): The communication link 3 failure means that only proportional parts in controller 3 and 4 are influenced, i.e., the proportional part of controller 3 is calculated according to the average of Δf_2 and Δf_3 and that of controller 4 is calculated according to Δf_4. The communication link 3 failure does not affect the integral part of each controller. Thus, the single communication failure has little affect on the frequency restoration, shown as Figs. 11(a) and (b).

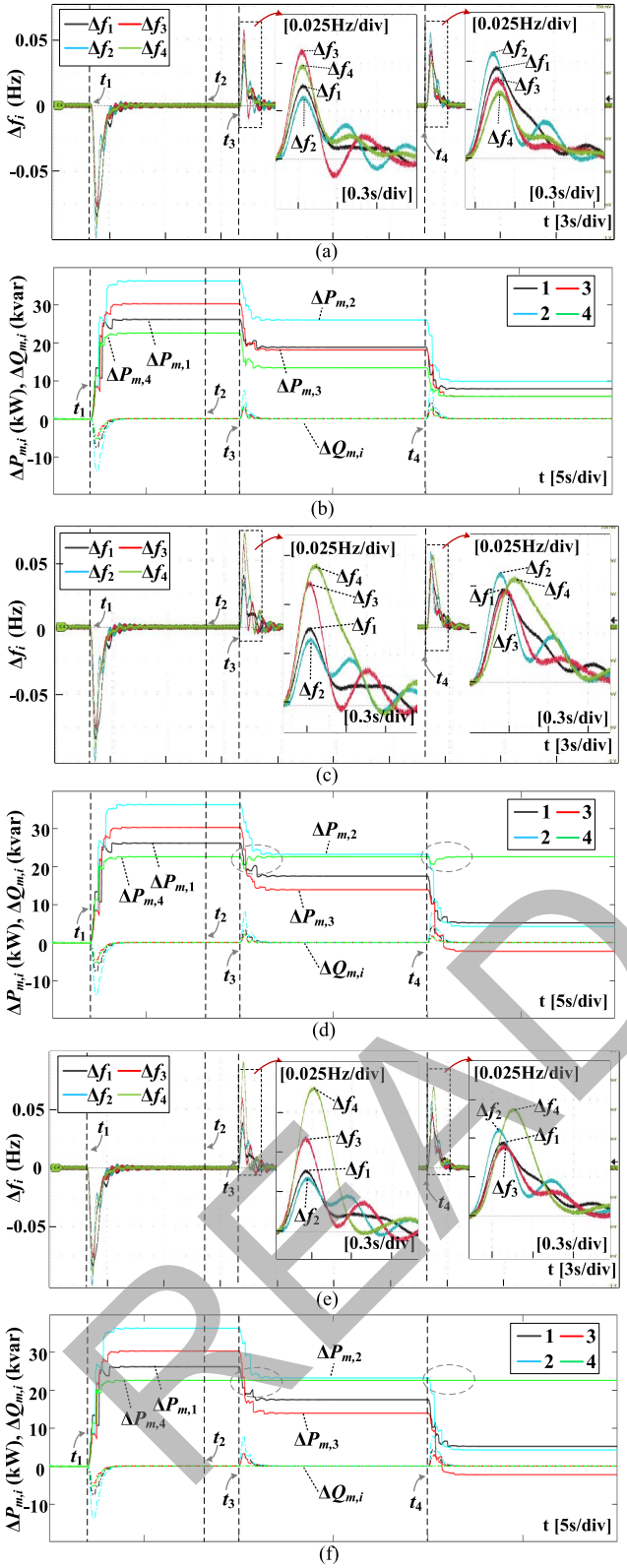

Fig. 11. Real-time experimental test: (a) frequency deviations of *Scenario 1*, (b) power corrections of *Scenario 1*, (c) frequency deviations of *Scenario 2*, (d) power corrections of *Scenario 2*, (e) frequency deviations of *Scenario 3*, (f) power corrections of *Scenario 3*.

Scenario 2 (Frequency measurement 4 failure occurs at $t = t_2$): The frequency measurement 4 failure means that the frequency deviation feedback of MG4 is fixed to $\Delta f_4 = 0$. It can be observed from Figs. 11(c) and (d) that the single frequency measurement failure dose not disturb the frequency deviations and power corrections if it occurs at the instant that frequency deviations are all 0. As the proportional part of each controller is calculated based on the average of neighboring frequency deviations, the proportional parts of controller 3 and 4 are smaller than the normal condition, which decelerates the frequency recovery of MG3 and MG4. As the integral part of each controller is calculated according to its local frequency deviation, the integral part of controller 4 are fixed to a constant value, so that the corresponding power corrections are only slightly influenced by the proportional part variation, shown as Fig. 11(d). But with the power corrections generated by other controllers, the frequency restoration can still be realized under loads and RES power disturbances.

Scenario 3 (Controller 4 failure occurs at $t = t_2$): The controller 4 failure means that the power corrections generated by controller 4 ($\Delta P_{m,4}$, $\Delta Q_{m,4}$) is fixed. It can be observed from Figs. 11(e) and (f) that the proposed control strategy can still realize the frequency restoration after the single controller failure. Even though power corrections from controller 4 are fixed, the frequency restoration can still be realized by adjusting power corrections in other microgrids and mutual power exchange among microgrids. It can also be observed that the single controller failure dose not disturb the frequency deviations and power corrections if it occurs when frequency deviations are all 0.

VI. Discussion

The objective of this paper was to introduce a robust secondary frequency control design method for the VSM-based MGC using equivalent modeling. Performance of the proposed control strategy was evaluated through simulation and real-time experiment, which shows good robustness against disturbances of loads and RES power, packet loss, and single communication link or controller failure. It is worth noting that the proposed secondary frequency control design method using equivalent modeling is not limited to the VSM-based MGC, but can also be extended to any type of LV or medium-voltage MGC. Any form of equivalent model for microgrids can be used to establish the simplified MGC model as long as it accurately fits the slow dynamics of actual microgrids. Modeling of unstructured uncertainties covering all the possible operating conditions and disturbances is a prerequisite to ensure the robustness of the designed controller.

VII. Conclusion

In this paper, a robust secondary frequency control design method using equivalent modeling is implemented in the VSM-based MGC system. To reduce the system model order, the EqSG model is used to formulate the nominal MGC model. To address modeling errors caused by equivalent modeling and different operating conditions, unstructured uncertainties are considered in the complete MGC model. The proposed control strategy is implemented in the distributed-centralized approach to exploit existent hierarchical control structure. The control parameters are designed using structured μ-synthesis

to satisfy robust performance. With the introduction of event-triggered mechanism, the transmission rate of signals among microgrids is greatly reduced without deteriorating robustness. Finally, the performance of the proposed control strategy is validated through simulation and real-time experiment.

APPENDIX

Parameters of the EqSG Model used in Section IV are $J_i^{eq} = 1.106(\mathrm{W{\cdot}s^3/rad^2})$, $D_{p,i}^{eq} = 71.25(\mathrm{W{\cdot}s^2/rad^2})$, $K_i^{eq} = 0.0046(\mathrm{var{\cdot}s/V})$, $D_{q,i}^{eq} = 2257(\mathrm{var/V})$, $r_i^{eq} = 0.0795(\Omega)$, $L_i^{eq} = 0.9682(\mathrm{mH})$, $r_{x,i}^{eq} = 0.6819$.

REFERENCES

[1] S. Peyghami, P. Palensky, and F. Blaabjerg, "An overview on the reliability of modern power electronic based power systems," *IEEE Open J. Power Electron.*, vol. 1, pp. 34–50, 2020.

[2] J. Liu, Y. Miura, H. Bevrani, and T. Ise, "Enhanced virtual synchronous generator control for parallel inverters in microgrids," *IEEE Trans. Smart Grid*, vol. 8, no. 5, pp. 2268–2277, Sep. 2017.

[3] J. A. Suul, S. D'Arco, and G. Guidi, "Virtual synchronous machine-based control of a single-phase bi-directional battery charger for providing vehicle-to-grid services," *IEEE Trans. Ind. Appl.*, vol. 52, no. 4, pp. 3234–3244, Jul./Aug. 2016.

[4] Q.-C. Zhong, "Power-electronics-enabled autonomous power systems: Architecture and technical routes," *IEEE Trans. Ind. Electron.*, vol. 64, no. 7, pp. 5907–5918, Jul. 2017.

[5] Y. Han, P. Shen, X. Zhao, and J. M. Guerrero, "Control strategies for islanded microgrid using enhanced hierarchical control structure with multiple current-loop damping schemes," *IEEE Trans. Smart Grid*, vol. 8, no. 3, pp. 1139–1153, May 2017.

[6] N. Pogaku, M. Prodanovic, and T. C. Green, "Modeling, analysis and testing of autonomous operation of an inverter-based microgrid," *IEEE Trans. Power Electron.*, vol. 22, no. 2, pp. 613–625, Mar. 2007.

[7] J. W. Simpson-Porco, Q. Shafiee, F. Dörfler, J. C. Vasquez, J. M. Guerrero and F. Bullo, "Secondary frequency and voltage control of islanded microgrids via distributed averaging," *IEEE Trans. Ind. Electron.*, vol. 62, no. 11, pp. 7025–7038, Nov. 2015.

[8] Y. Xu, H. Sun, W. Gu, Y. Xu, and Z. Li, "Optimal distributed control for secondary frequency and voltage regulation in an islanded microgrid," *IEEE Trans. Ind. Informat.*, vol. 15, no. 1, pp. 225–235, Jan. 2019.

[9] H. Bevrani, M. R. Feizi, and S. Ataee, "Robust frequency control in an islanded microgrid: H_∞ and μ -synthesis approaches," *IEEE Trans. Smart Grid*, vol. 7, no. 2, pp. 706–717, Mar. 2016.

[10] C. Peng, J. Zhang, and H. Yan, "Adaptive event-triggering H_∞ load frequency control for network-based power systems," *IEEE Trans. Ind. Electron.*, vol. 65, no. 2, pp. 1685–1694, Feb. 2018.

[11] Md. Rasheduzzaman, J. A. Mueller, and J. W. Kimball, "Reduced-order small-signal model of microgrid systems," *IEEE Trans. Sustain. Energy*, vol. 6, no. 4, pp. 1292–1305, Oct. 2015.

[12] Z. Shuai, Y. Peng, X. Liu, Z. Li, J. M. Guerrero, and Z. J. Shen, "Dynamic equivalent modeling for multi-microgrid based on structure preservation method," *IEEE Trans. Smart Grid*, vol. 10, no. 4, pp. 3929–3942, Jul. 2019.

[13] W. Hu, Z. Wu, and V. Dinavahi, "Dynamic analysis and model order reduction of virtual synchronous machine based microgrid," *IEEE Access*, vol. 8, pp. 106585–106600, 2020.

[14] D. I. Brandao, T. Caldognetto, F. P. Marafão, M. G. Simões, J. A. Pomilio, and P. Tenti, "Centralized control of distributed single-phase inverters arbitrarily connected to three-phase four-wire microgrids," *IEEE Trans. Smart Grid*, vol. 8, no. 1, pp. 437–446, Jan. 2017.

[15] Y. Han, K. Zhang, H. Li, E. A. A. Coelho, and J. M. Guerrero, "MAS-based distributed coordinated control and optimization in microgrid and microgrid clusters: A comprehensive overview," *IEEE Trans. Power Electron.*, vol. 33, no. 8, pp. 6488–6508, Aug. 2018.

[16] A. Bani-Ahmed, M. Rashidi, A. Nasiri, and H. Hosseini, "Reliability analysis of a decentralized microgrid control architecture," *IEEE Trans. Smart Grid*, vol. 10, no. 4, pp. 3910–3918, Jul. 2019.

[17] Y. Han, H. Li, L. Xu, X. Zhao, and J. M. Guerrero, "Analysis of washout filter-based power sharing Strategy—An equivalent secondary controller for islanded microgrid without LBC lines," *IEEE Trans. Smart Grid*, vol. 9, no. 5, pp. 4061–4076, Sep. 2018.

[18] Y. Khayat *et al.*, "On the secondary control architectures of AC microgrids: An overview," *IEEE Trans. Power Electron.*, vol. 35, no. 6, pp. 6482–6500, Jun. 2020.

[19] H.-J. Yoo, T.-T. Nguyen, and H.-M. Kim, "Consensus-based distributed coordination control of hybrid AC/DC microgrids," *IEEE Trans. Sustain. Energy*, vol. 11, no. 2, pp. 629–639, Apr. 2020.

[20] A. Fathi, Q. Shafiee, and H. Bevrani, "Robust frequency control of microgrids using an extended virtual synchronous generator," *IEEE Trans. Power Syst.*, vol. 33, no. 6, pp. 6289–6297, Nov. 2018.

[21] H. R. Baghaee, M. Mirsalim, G. B. Gharehpetian, and H. A. Talebi, "A decentralized robust mixed H_2/H_∞ voltage control scheme to improve small/large-signal stability and FRT capability of islanded multi-DER microgrid considering load disturbances," *IEEE Syst. J.*, vol. 12, no. 3, pp. 2610–2621, Sep. 2018.

[22] J. Lai, X. Lu, X. Yu, and A. Monti, "Stochastic distributed secondary control for AC microgrids via event-triggered communication," *IEEE Trans. Smart Grid*, vol. 11, no. 4, pp. 2746–2759, Jul. 2020.

[23] K. Zhou and J. C. Doyle, *Essentials of Robust Control*. Upper Saddle River, NJ, USA: Prentice-Hall, 1998, pp. 130–137.

[24] S. Papathanassiou, N. Hatziargyriou, and K. Strunz, "A benchmark low voltage microgrid network," in *Proc. CIGRE Symp.*, Apr. 2005, pp. 1–8.

[25] E. A. Coelho *et al.*, "Small-signal analysis of the microgrid secondary control considering a communication time delay," *IEEE Trans. Ind. Electron.*, vol. 63, no. 10, pp. 6257–6269, Oct. 2016.

[26] H. R. Baghaee, M. Mirsalim, G. B. Gharehpetian, and H. A. Talebi, "A generalized descriptor-system robust H_∞ control of autonomous microgrids to improve small and large signal stability considering communication delays and load nonlinearities," *Int. J. Elect. Power Energy Syst.*, vol. 92, pp. 63–82, Nov. 2017.

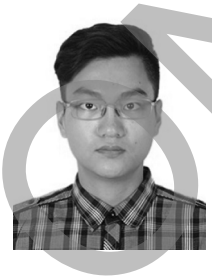

Wenqiang Hu (Student Member, IEEE) received the B.Eng. degree in electrical engineering and its automation from the China University of Petroleum (East China), Qingdao, China, in 2015. He is currently pursuing the Ph.D. degree in electrical engineering with Southeast University, Nanjing, China. From 2019 to 2020, he was a joint Ph.D student with the RTX Lab, University of Alberta, Edmonton, AB, Canada. His research interests include power electronics control, distributed generation, and microgrid.

Zaijun Wu (Member, IEEE) received the B.Eng. degree in power system and its automation from the Hefei University of Technology, Hefei, China, in 1996, and the Ph.D. degree in electrical engineering from Southeast University, Nanjing, China, in 2004. From 2012 to 2013, he was a Visiting Scholar with Ohio State University, Columbus, OH, USA. He is currently a Professor in electrical engineering with the School of Electrical Engineering, Southeast University. He has authored or coauthored more than 130 referred journal papers, and a reviewer of several journals. His research interests include microgrid, active distribution network, and power quality.

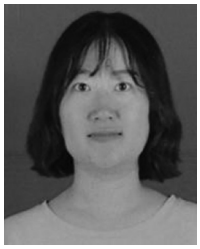

Xinxin Lv (Student Member, IEEE) received the B.S. degree in mathematics from Ludong University in 2015. She is currently pursuing the Ph.D. degree in electrical engineering with Hohai University, China. In 2019 and 2020, she was a joint Ph.D. student with RTX Lab, University of Alberta, Edmonton, AB, Canada. Her research interests include power system modeling and application, stability analysis and control of power systems, and load frequency control of power system.

Venkata Dinavahi (Fellow, IEEE) received the B.Eng. degree in electrical engineering from the Visvesvaraya National Institute of Technology, Nagpur, India, in 1993, the M.Tech. degree in electrical engineering from the Indian Institute of Technology Kanpur, India, in 1996, and the Ph.D. degree in electrical and computer engineering from the University of Toronto, ON, Canada, in 2000. He is currently a Professor with the Department of Electrical and Computer Engineering, University of Alberta, Edmonton, AB, Canada. His research interests include real-time simulation of power systems and power electronic systems, electromagnetic transients, devicelevel modeling, large-scale systems, and parallel and distributed computing.